Partial Wave Analysis of $\Xi_c^+ \to \Xi^- \pi^+ \pi^+$ at Belle and Belle II

S. X. Li, S. S. Tang, C. P. Shen, R. G. Ping

Zhengzhou University

Belle II China @ Belle II

2025/08/27

Motivation

- **$\Xi_c^+ \to \Xi^-\pi^+\pi^-$ is a golden channel to study properties of the excited Ξ^* states.**

➢ Belle has reported a research on this process in 2019 based on a 980 fb^{-1} data sample. The first observation of the $\Xi(1620)^0$ and the 4.0σ evidence of the $\Xi(1690)^0$ were reported. An unknown structure in the range 1.8–2.1 GeV/c^2 in the $M(\Xi^-\pi^+)$ was seen, which has been expected to be due to resonances such as $\Xi(1820)^0$, $\Xi(1950)^0$, and $\Xi(2030)^0$.

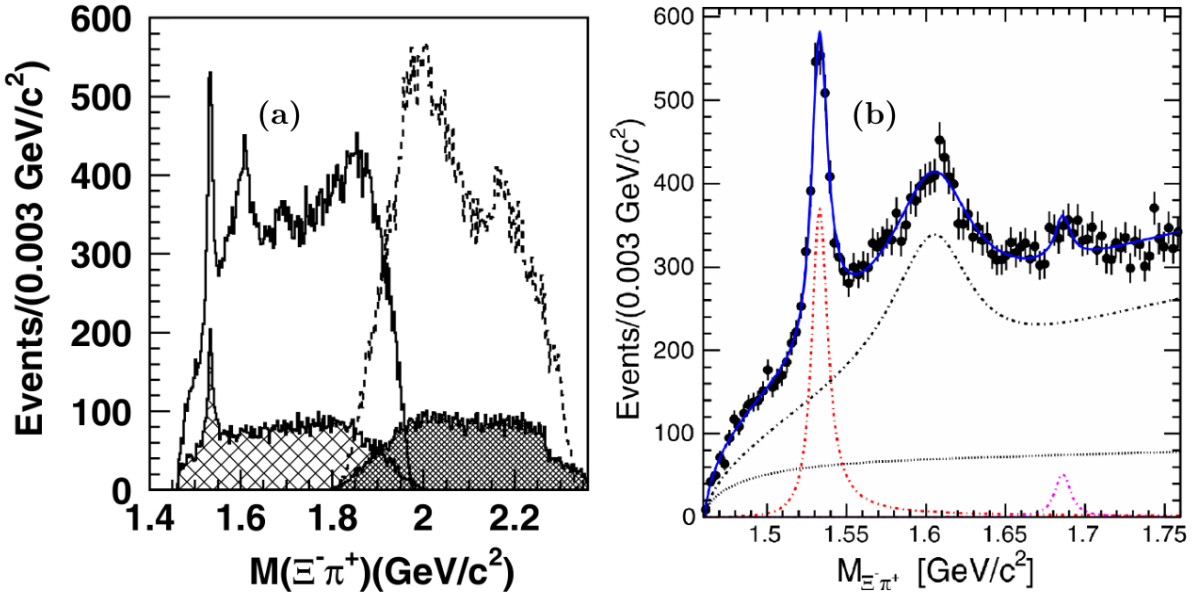

Phys. Rev. Lett 122 072501 (2019)

➢ The spin-parities of $\Xi(1620)^0$, $\Xi(1950)^0$, and $\Xi(2030)^0$ have not been determined yet.

- **Partial wave analysis is one of the best techniques to study the internal dynamics of three-body decays and the large statistic of $\Xi_c^+ \to \Xi^-\pi^+\pi^-$ in Belle (II) makes the partial wave analysis possible.**

Datasets

- **Belle and Belle II (Run I) data samples:**

TABLE I: Integrated luminosities of Belle and Belle II data samples in the unit of fb^{-1} used in this analysis.

	$\Upsilon(1S,\ 2S,\ 3S)$	Below $\Upsilon(4S)$	$\Upsilon(4S)$	Above $\Upsilon(4S)$	Sum
Belle	33.5	89.5	711.0	149.0	983
Belle II	$\cdots$	42.6	364.1	19.8	427

- **Belle and Belle II generic MC samples:**

  - Four streams of Belle official generic MC samples: $\Upsilon(1S,\ 2S,\ 3S)$ decays, $\Upsilon(4S) \to B^+B^-/B^0\bar{B}^0$, $\Upsilon(5S) \to B^{(*)}_{(s)}\bar{B}^{(*)}_{(s)}$, and $e^+e^- \to q\bar{q}$ $(q = u,\ d,\ s,\ c)$ at e^+e^- C.M. energies of 10.52, 10.58, and 10.867 GeV.

  - Belle II official MC16rd generic MC samples: $1444/267/77\,\text{fb}^{-1}$ collected at on/below/above $\Upsilon(4S)$-resonance.

Datasets

- **Belle and Belle II signal MC samples:**

1. Decay process: $e^+e^- \to c\bar{c} \to \Xi_c^+ + X,\ \Xi_c^+ \to \Xi^-\pi^+\pi^+, \Xi^- \to \Lambda\pi^-, \Lambda \to p\pi^-$
2. Run-dependent signal MC sample for Belle II
3. run-dependent signal MC sample for Belle
4. Generated number: 10,000,000 for each

- **Software version:**

1. Belle: B2BII (light-2503-ceres)
2. Belle II: BASF2 (light-2503-ceres)

Event selection

Optimization method:

The selection criteria are optimized based on figure-of-merit (FOM), defined as:

$$FOM = \frac{\epsilon}{5/2 + \sqrt{B}}$$

ϵ is the signal efficiency obtained from signal MC samples;

B is the number of background events in the Ξ_c^+ signal region, estimated from the generic MC samples.

The Ξ_c^+ signal region: ~~$|M(\Xi^-\pi^+\pi^+) - m(\Xi_c^+)| < 15\ \mathrm{MeV}/c^2$~~ $2.46 < M(\Xi^-\pi^+\pi^+) < 2.48\ \mathrm{GeV}/c^2$ (reduce background level)

The Ξ_c^+ sideband regions: ~~37~~ 35 $< |M(\Xi^-\pi^+\pi^+) - m(\Xi_c^+)| <$ ~~67~~ 55 MeV/ c^2 (twice larger than signal region)

The selection criteria are similar as those in B2N: BELLE2-PUB-PH-2025-002 (Measurements of $\Xi_c^+ \to \Sigma^+ K_S^0 / \Xi^0\pi^+ / \Xi^0 K^+ / \Xi^-\pi^+\pi^+$)

Event selection

- π^+: from good charged tracks:
  - $17° < \theta < 150°$, where θ is the polar angle of the track.
  - $dr < 0.2$ cm and $|dz| < 1.0$ cm, where dr and dz are impact parameters perpendicular to and along the beam direction with respect to the interaction point (IP).
  - $\frac{\mathcal{L}(\pi)}{\mathcal{L}(\pi)+\mathcal{L}(K)} > 0.6$ and $\frac{\mathcal{L}(\pi)}{\mathcal{L}(\pi)+\mathcal{L}(p)} > 0.6$, where $\mathcal{L}(i)$ is the likelihood for the particle identification ($i = \pi$, p or K) that is combined from the information from different detector subsystems.
- $\Lambda \to p\pi^-$: selected from "stdLambdas"
  - $chiProb > 0$, where $chiProb$ is the probability of vertex fit on Λ.
  - $\cos\theta > 0.0$, where θ is the angle between Λ momentum and the vertex vector from IP.
  - $\sqrt{dr^2 + dz^2} > 0.35$ cm
  - $\frac{\mathcal{L}(p)}{\mathcal{L}(p)+\mathcal{L}(\pi)} > 0.2$ and $\frac{\mathcal{L}(p)}{\mathcal{L}(p)+\mathcal{L}(K)} > 0.2$ for Belle; $protonID > 0.01$ for Belle II, where $protonID$ is defined as $\frac{L(p)}{L(\pi)+L(K)+L(p)+L(e)+L(\mu)}$.
  - $|M(p\pi^-) - m(\Lambda)| < 3.5$ MeV/c^2, where $m(\Lambda)$ is the nominal Λ mass.

Event selection

- $\Xi^- \to \Lambda\pi^-$: "goodXi:loose" from "stdHyperons"
  - $chiProb > 0$ for a vertex fit on Ξ^-.
  - $\cos\theta > 0.0$, where θ is the angle between Ξ^- momentum and the vertex vector from IP.
  - $\sqrt{dr^2 + dz^2} > 0.1$ cm and $\sqrt{dr^2 + dz^2} < \sqrt{dr^2(\Lambda) + dz^2(\Lambda)}$.
  - $p_t(\pi^-) > 0.05$ GeV and $\frac{\cos\theta(\Lambda)}{\cos\theta(\Xi^-)} < 1.006$, where θ is the angle between momentum and vertex vector (vector connecting IP and fitted vertex) of this particle in xy-plane.
  - $|M(\Lambda\pi) - m(\Xi^-)| < 4.5$ MeV/c^2 ($\approx \pm 2\sigma$), where $m(\Xi^-)$ is the nominal Ξ^- mass.

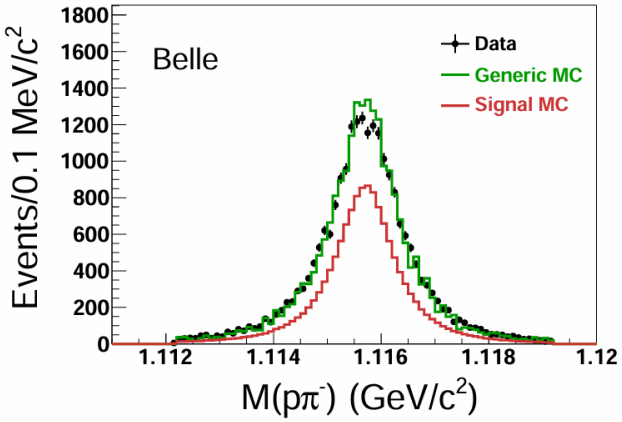

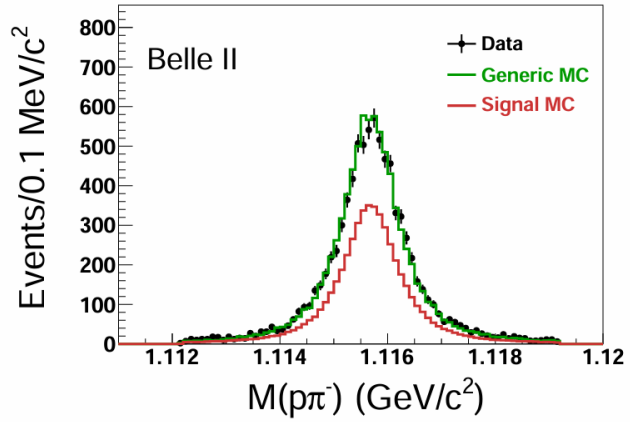

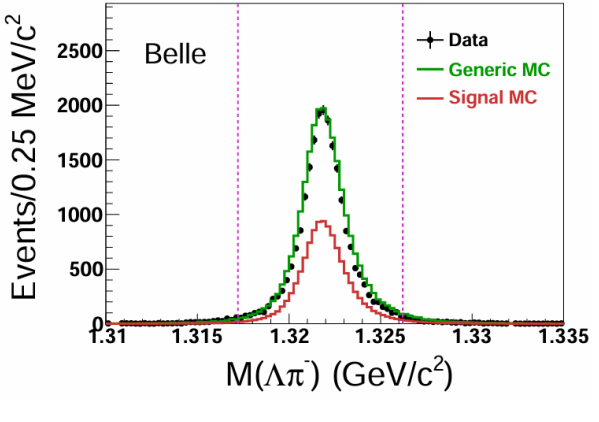

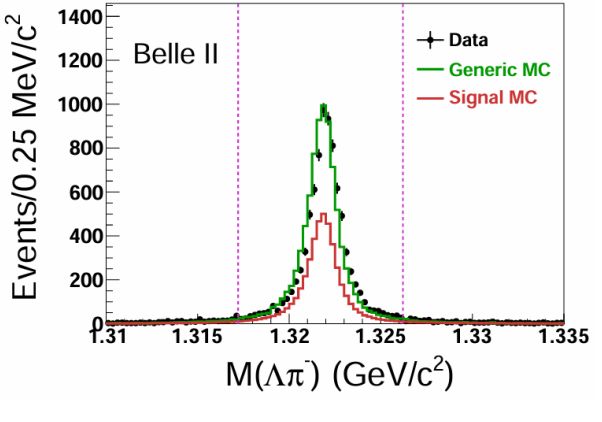

Event selection

- $\Xi_c^+ \to \Xi^-\pi^+\pi^+$:

  - $x_p > 0.6$, where $x_p = p_{\rm cm}/p_{\rm max}$ is the scaled momentum of the Ξ_c^+. Here, $p_{\rm cm}$ is the Ξ_c^+ momentum in the e^+e^- center-of-mass frame and $p_{\rm max} = \sqrt{s/4 - M^2}$, where s is the total center-of-mass energy square and M is the invariant mass of the $\Xi^-\pi^+\pi^+$.

  - $\chi^2(\Xi_c^+) < 20$, where $\chi^2(\Xi_c^+)$ is the vertex fit quality on Ξ_c^+. We use "treeFit" to make the vertex fit and require the Λ and Ξ^- masses constrained to their nominal masses.

  - $L/\sigma_L(\Xi_c^+) > 2.0$, where $L/\sigma_L(\Xi_c^+)$ is the significance of the Ξ_c^+ flight distance, defined as the distance between the IP and decay vertex divided by the uncertainty on this distance.

The above three cuts are all optimized.

Event selection

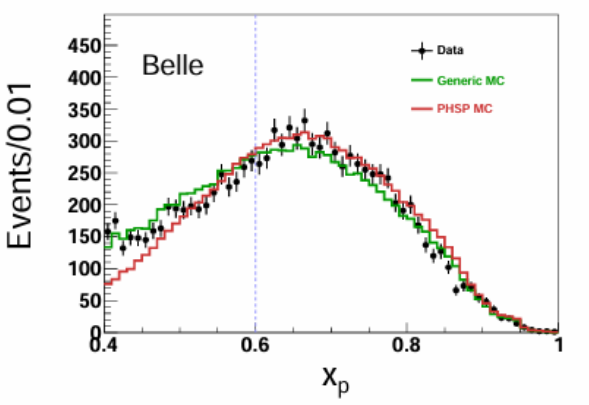

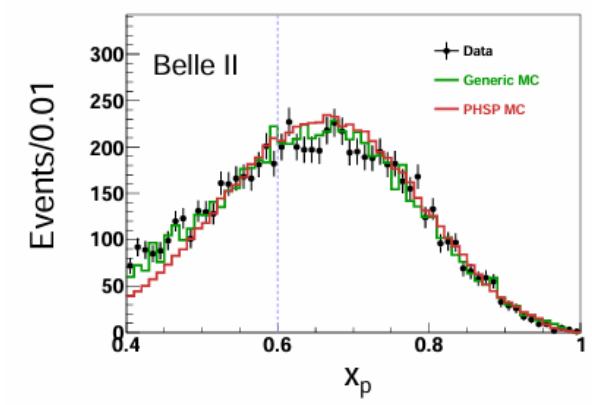

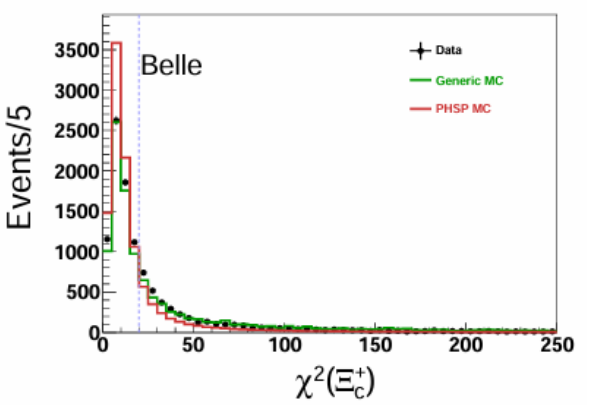

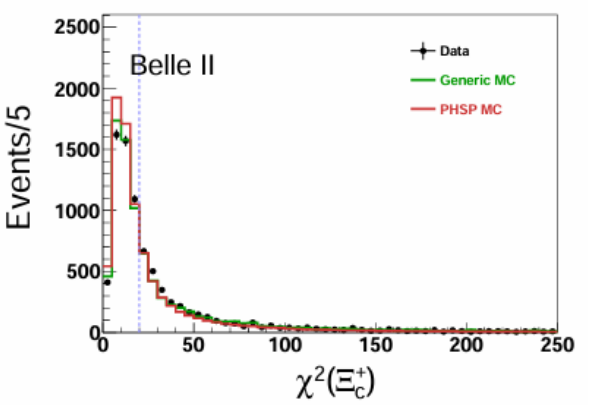

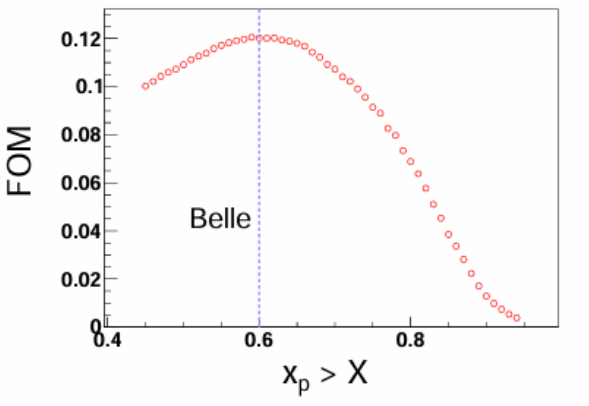

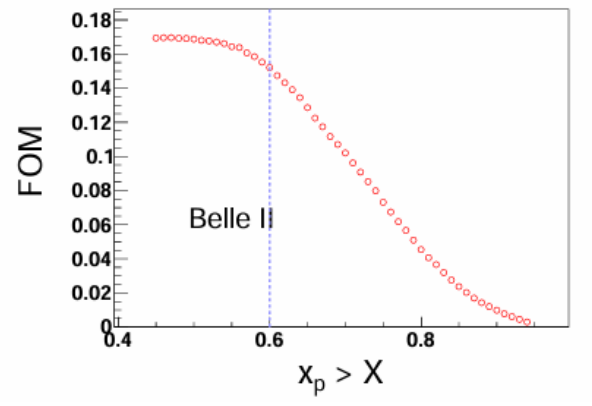

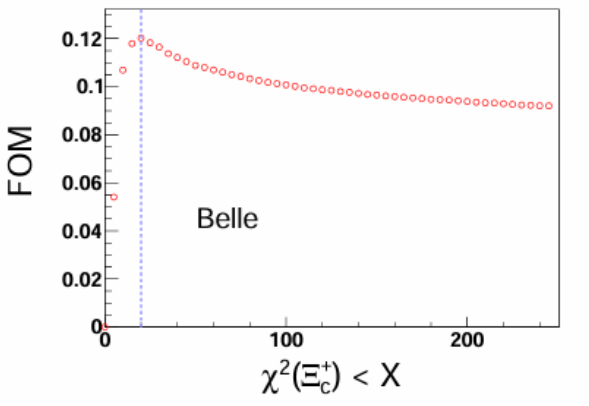

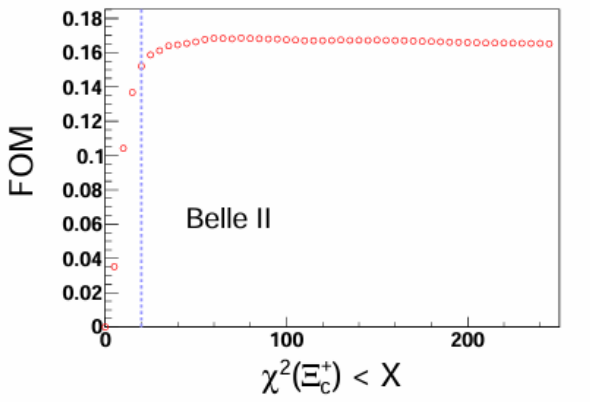

$x_p > 0.6$

$\chi^2(\Xi_c^+) < 20$

Event selection

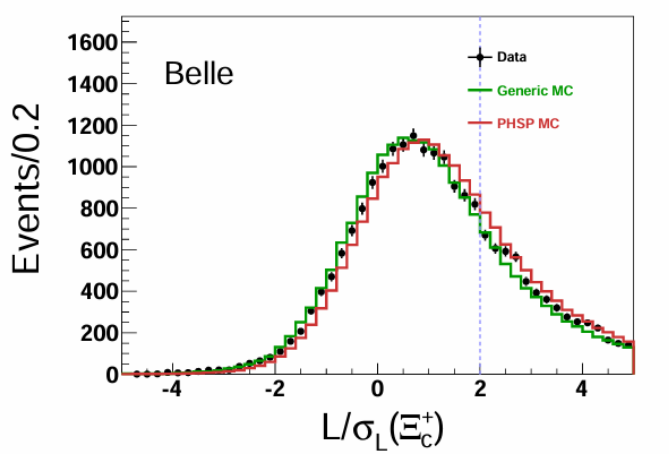

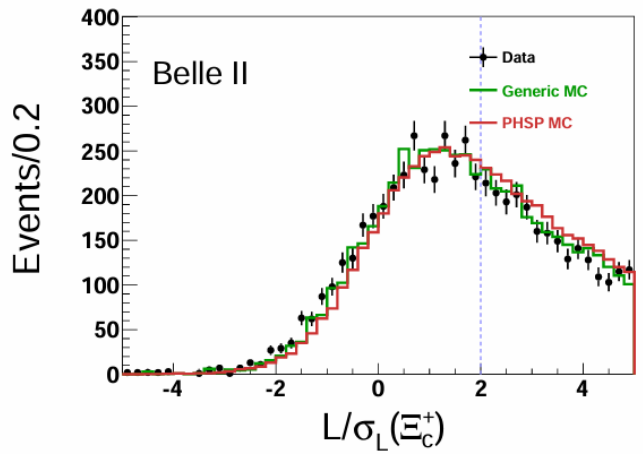

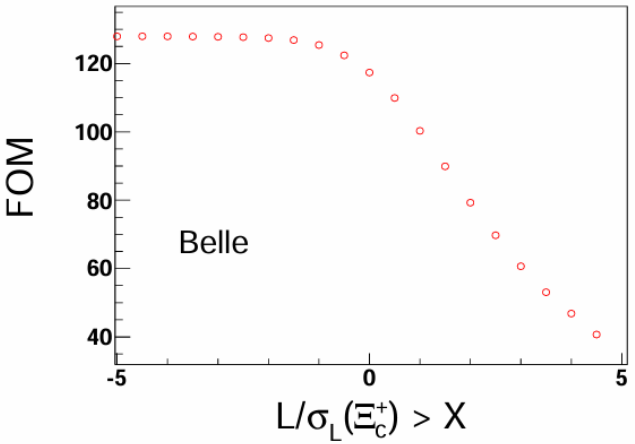

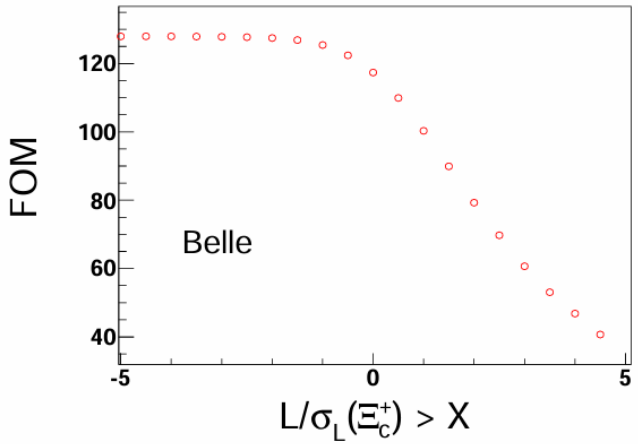

- Note that the optimized cut is $\boldsymbol{L/\sigma_L(\Xi_c^+) > 0.0}$.
- Considering the low background level required by the PWA (< 5%, the lower the background level, the better the PWA results), we adopt the $\boldsymbol{L/\sigma_L(\Xi_c^+) > 2.0}$, reducing the background level from 11% to 4%.

cuts:

$L/\sigma > X$		> 0.0	> 0.5	> 1.0	> 1.5	> 2.0	> 2.5	> 3.0
Belle	bkglev (%)	12.0	10.4	8.7	6.0	3.9	3.2	2.8
	ϵ (%)	4.3	3.7	3.0	2.4	1.8	1.4	1.0
Belle II	bkglev (%)	10.1	8.3	6.6	5.1	3.1	2.7	2.2
	ϵ (%)	4.5	4.1	3.9	3.5	3.0	2.8	2.4

Background Study

- no peaking background contributed in the Ξ_c^+ signal region
- Invariant mass distribution of $\Xi^-\pi^+\pi^+$ from data for Belle (left) and Belle II (right)
- Fit to the M($\Xi^-\pi^+\pi^+$) distributions: double-Gaussian function (signal) + first-order polynomial (background).

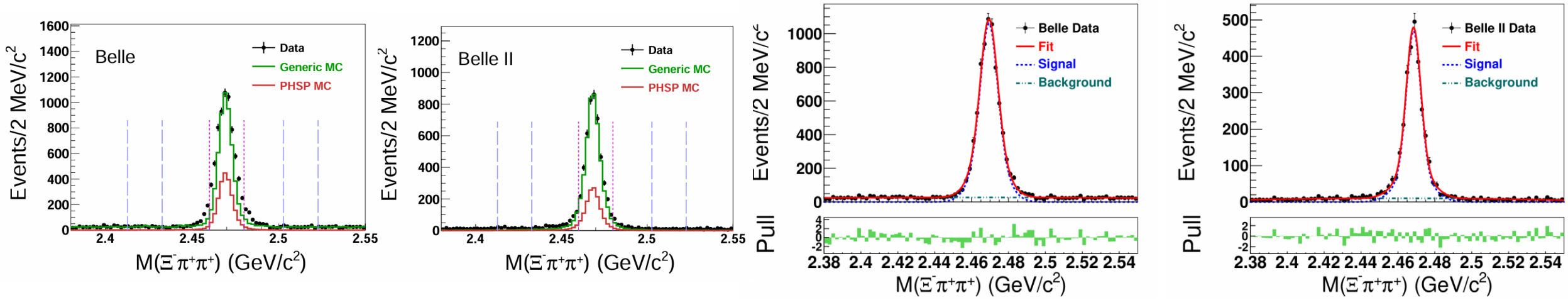

The fitted signal yields and the fitted background events in the Ξ_c^+ signal region for Belle and Belle II datasets.

	N_{Signal}	$N_{\text{Background}}$	Background Level
Belle	6465 ± 86	265 ± 18	3.9%
Belle II	4540 ± 75	147 ± 12	3.1%

Cross check for Belle and Belle II

We also compare the $\frac{N_{\rm sig}}{\mathcal{L}_{\rm int}\epsilon^{\rm MC}}$ for Belle and Belle II, and we find they are consistent with each other.

	$N_{\rm sig}$	$\mathcal{L}_{\rm int}(\rm fb^{-1})$	$\epsilon^{\rm MC}$ (%)	$\frac{N_{\rm sig}}{\mathcal{L}_{\rm int}\epsilon^{\rm MC}}$ $(\frac{1}{\rm fb^{-1}})$
Belle	6545 ± 86	980	1.81	364.2 ± 4.8
Belle II	4540 ± 75	427	3.03	350.3 ± 5.8

Kinematic Distributions

- We check the kinematic distributions from data in the Ξ_c^+ sideband, generic MC samples in the Ξ_c^+ signal region and sideband, and PHSP MC samples in the Ξ_c^+ signal region.
- The distributions from data in the Ξ_c^+ signal region will be given here after we open the box.

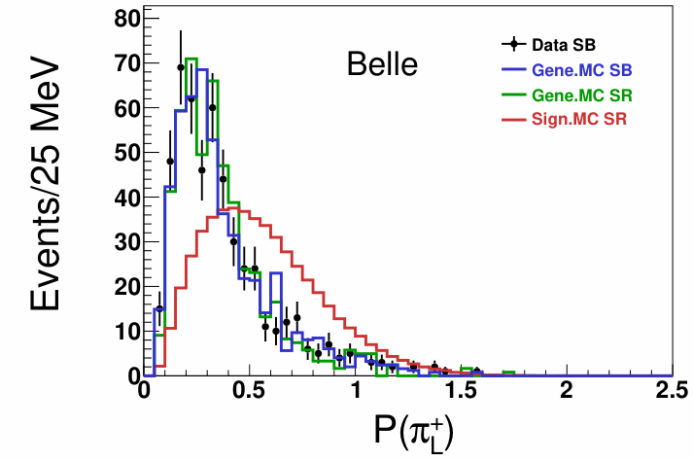

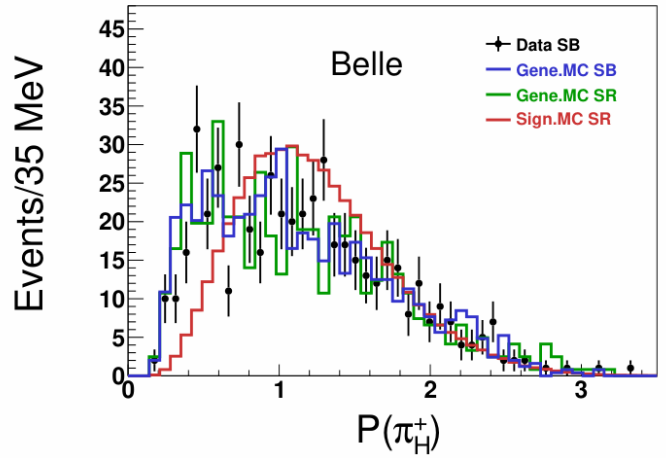

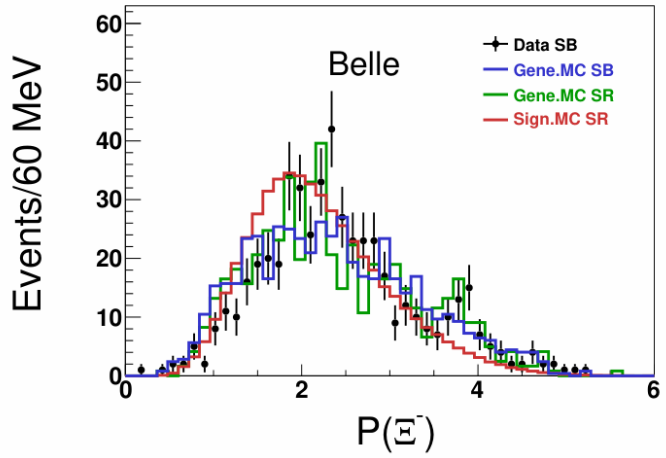

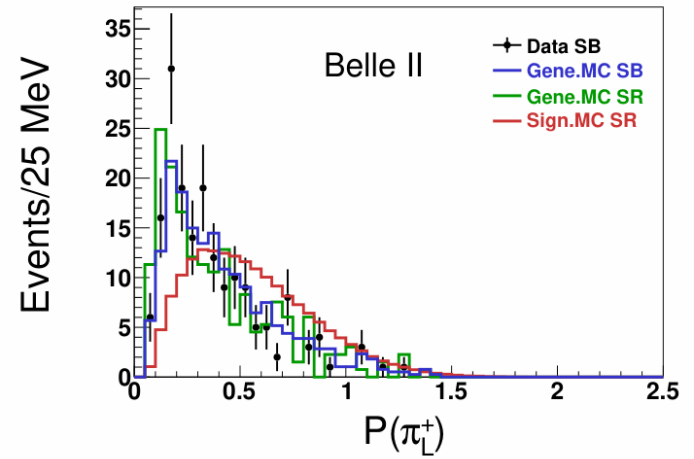

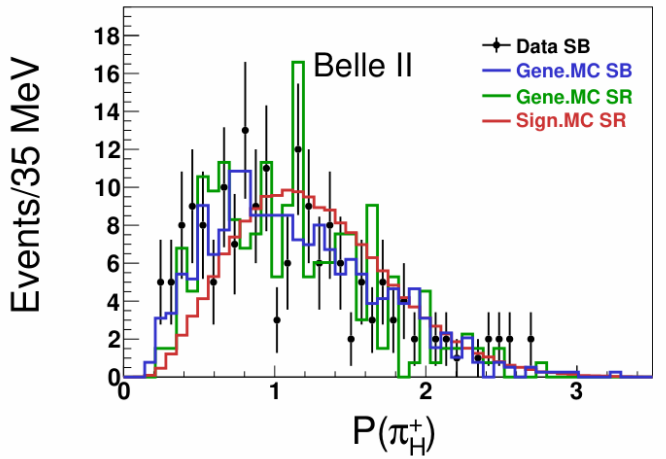

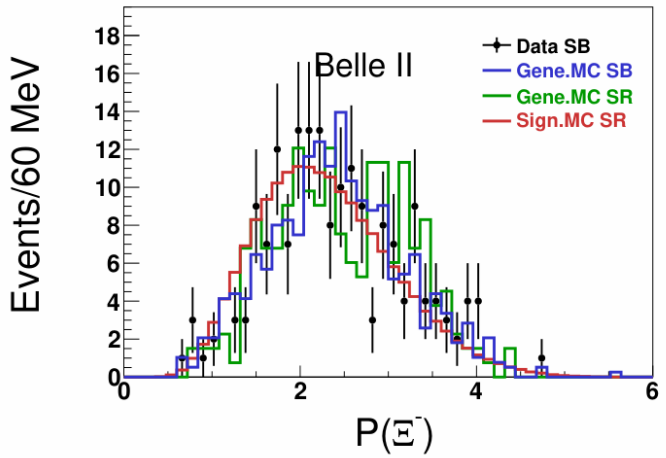

Kinematic Distributions

- We check the kinematic distributions from data in the Ξ_c^+ sideband, generic MC samples in the Ξ_c^+ signal region and sideband, and PHSP MC samples in the Ξ_c^+ signal region.
- The distributions from data in the Ξ_c^+ signal region will be given here after we open the box.

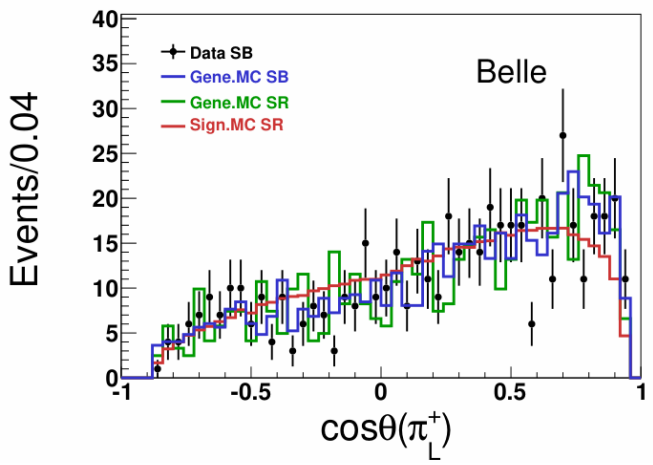

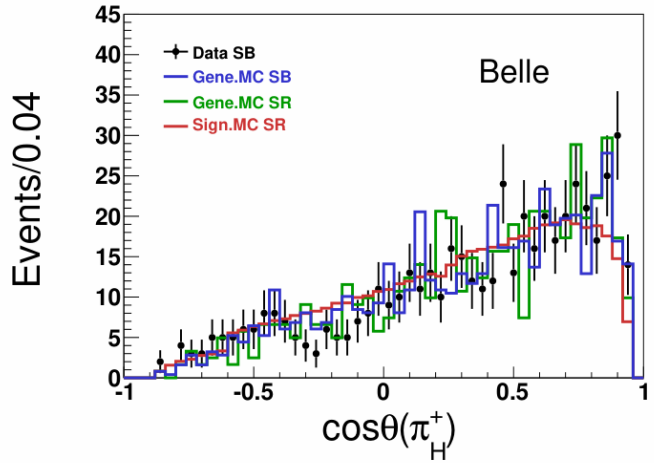

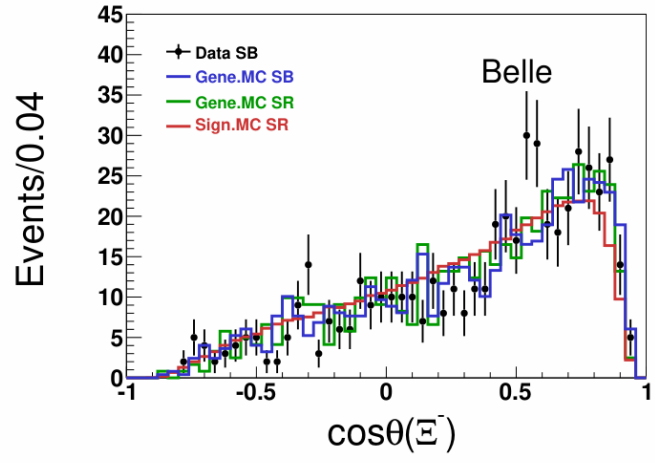

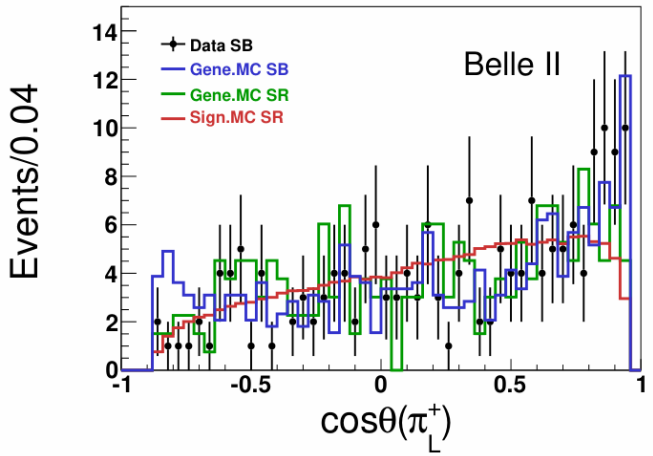

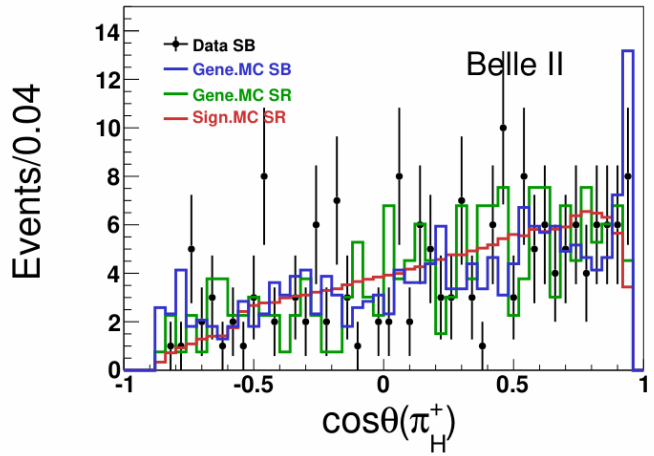

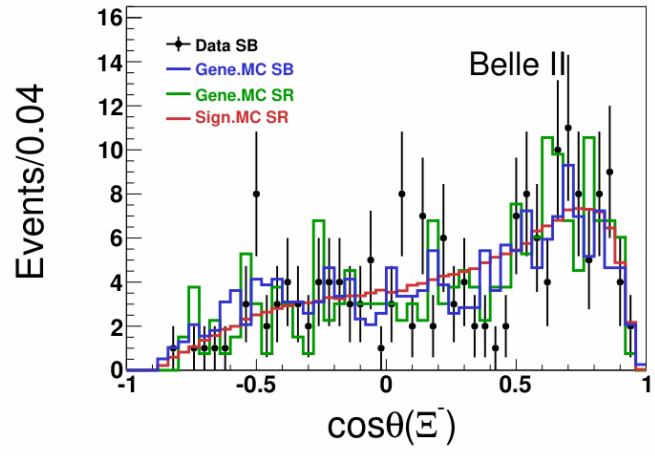

Kinematic Distributions

- We check the kinematic distributions from data in the Ξ_c^+ sideband, generic MC samples in the Ξ_c^+ signal region and sideband, and PHSP MC samples in the Ξ_c^+ signal region.
- The distributions from data in the Ξ_c^+ signal region will be given here after we open the box.

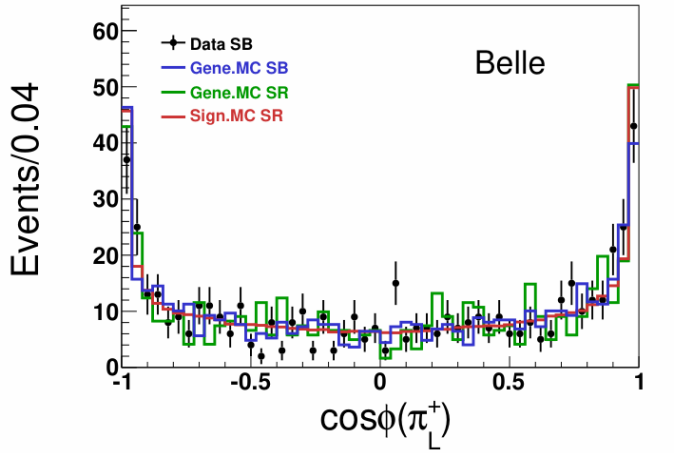

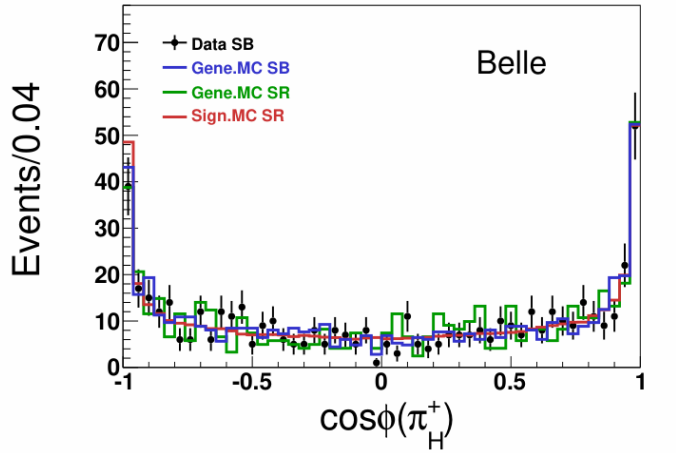

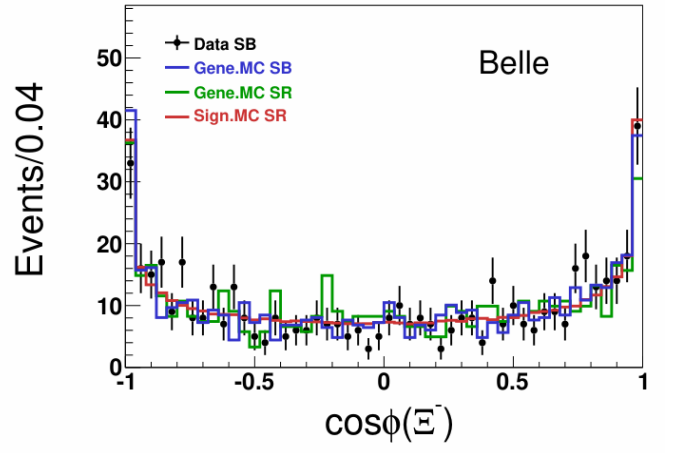

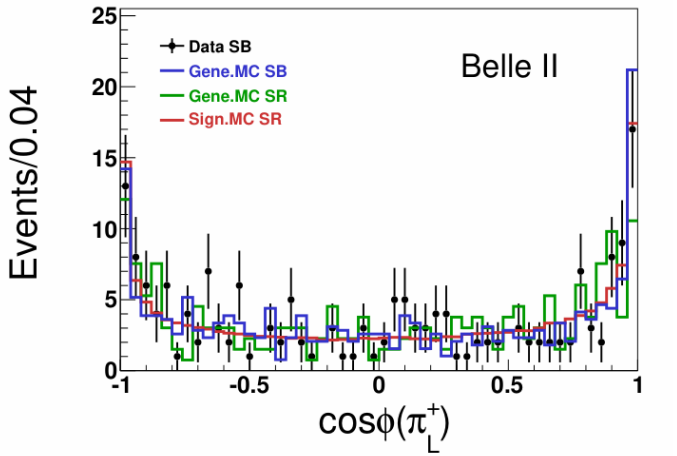

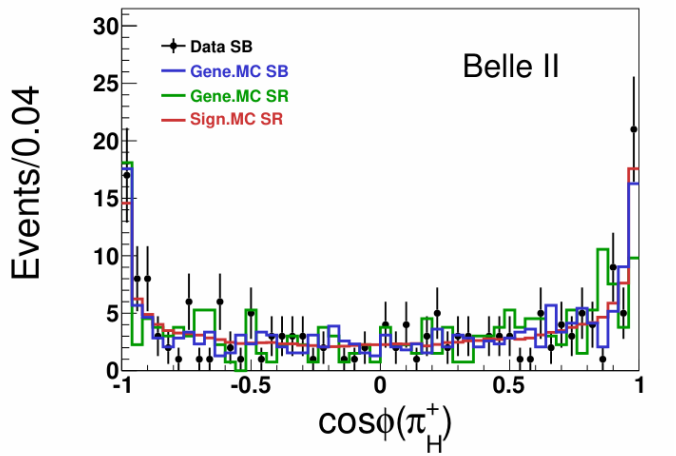

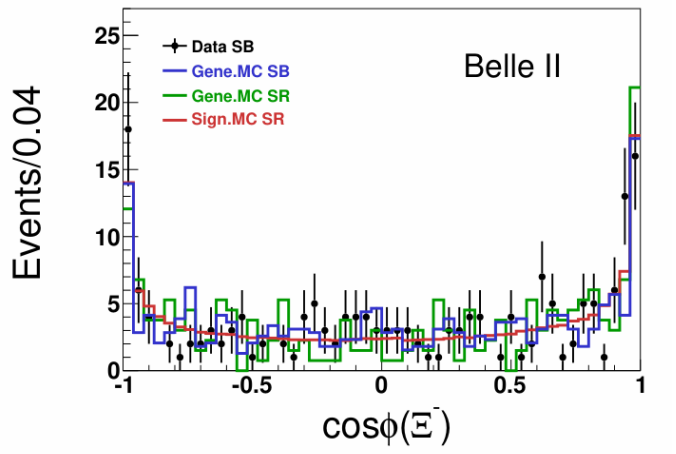

Kinematic Distributions

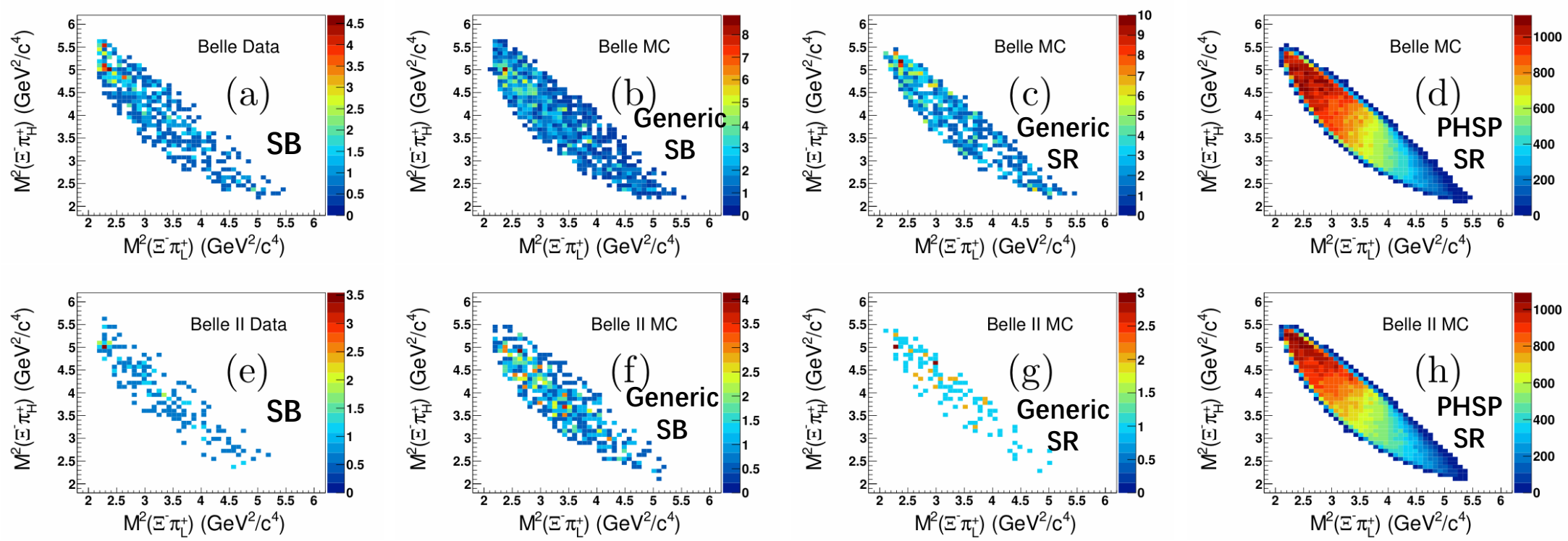

Figure 9: Dalitz plots of $M^2(\Xi^-\pi_H^+)$ versus $M^2(\Xi^-\pi_L^+)$ from data in the Ξ_c^+ SB (a,e), generic MC in the Ξ_c^+ SB (b,f), generic MC in the Ξ_c^+ SR (c,g), and PHSP MC in the Ξ_c^+ SR (d,h) for Belle (upper) and Belle II (bottom).

Kinematic Distributions

Projections of Dalitz plots

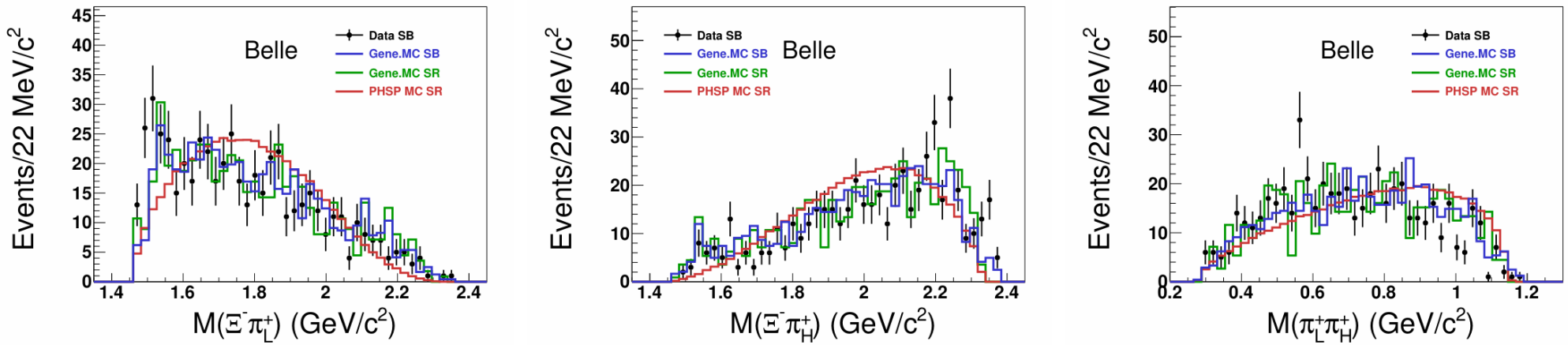

- The size of the phase space of the SB is larger than that of the SR.
- However the kinematic distributions from data in SB and generic MC in SB and SR are consistent.
- Thus we use the normalized generic MC events in the SR to describe the background events in data in the SR.

Partial Wave Analysis (PWA)

Decay Amplitude

The Feynman diagrams for the process $\Xi_c^+ \to \Xi^*\pi^+;\ \Xi^* \to \Xi^-\pi^+$ are shown as below.

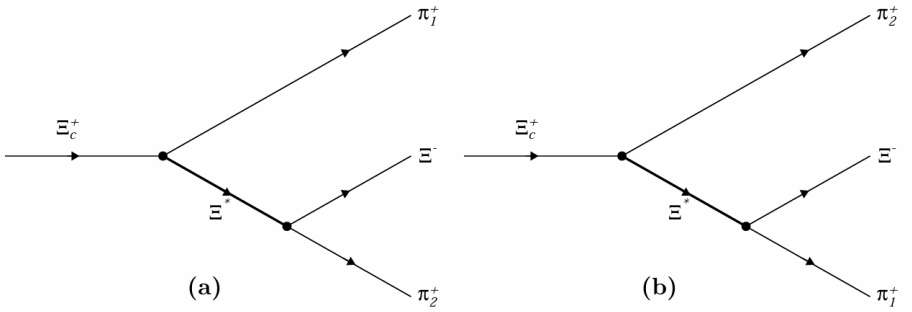

The decay amplitude for this process is constructed using the covariant tensor formalism [Eur. Phys. J. A 16, 537 (2003)], which is written as:

$$M_i = \bar{u}(p_{\Xi^-}, \lambda_{\Xi^-}) V_{\Xi^*\to\Xi^-\pi^+} G_{\Xi^*}^{(J^P)} V_{\Xi_c^+\to\Xi^*\pi^+} u(p_{\Xi_c^+}, \lambda_{\Xi_c^+}),$$

u is the spinor for a baryon,

V is the effective vertex,

G is the propagator of the Ξ^* resonance,

p is the four-momentum, and λ is the third component of the spin projection.

Collaborate with Ronggang Ping
(Institute of High Energy Physics)

The spinor for a spin-1/2 baryon is expressed as:

$$u(\vec{p},\lambda) = \begin{pmatrix} \sqrt{E+m} \\ \frac{\vec{\sigma}\cdot\vec{p}}{\sqrt{E+m}} \end{pmatrix} \chi(\lambda), \tag{1}$$

where m, E, and $\vec{p}$ are the mass, energy, and momentum of the baryon, respectively, $\vec{\sigma}$ is the pauli vector, and $\chi(\lambda)$ is the spin wave-function for a baryon. The projection operator for a spin-1/2 baryon is defined as:

$$\mathcal{P}^{(\frac{1}{2})} = \sum_{\lambda} u(\vec{p},\lambda)\bar{u}(\vec{p},\lambda) = \not{p} + m, \tag{2}$$

where $\not{p} \equiv \gamma^{\mu} p_{\mu}$. The spinor for a spin-$(n+\frac{1}{2})$ baryon ($n = 1,\ 2,\ 3,\ ...$) can be obtained using the polarization vector and the Clebsch-Gordan coefficient, as follows:

$$\begin{aligned} U_{\mu_1\mu_2\ldots\mu_n}(\vec{p},\lambda) &= \sum_{\lambda_n,\lambda_{n+1}} \left\langle n,\lambda_n;\frac{1}{2},\lambda_{n+1}|n+\frac{1}{2},\lambda\right\rangle \epsilon_{\mu_1\mu_2\ldots\mu_n}(\vec{p},\lambda_n)u(\vec{p},\lambda_{n+1}), \\ \epsilon_{\mu_1\mu_2\ldots\mu_n}(\vec{p},\lambda) &= \sum_{\lambda_{n-1},\lambda_n} \langle n-1,\lambda_{n-1};1,\lambda_n|n,\lambda\rangle\, \epsilon_{\mu_1\mu_2\ldots\mu_{n-1}}(\vec{p},\lambda_{n-1})\epsilon_{\mu_n}(\vec{p},\lambda_n), \end{aligned} \tag{3}$$

where $\epsilon_{\mu_n}(\vec{p},\lambda_n)$ is the polarization vector. The wave function satisfies the Rarita-Schwinger conditions [**?**]. The projection operator for a spin-$(n+\frac{1}{2})$ baryon ($n = 1,\ 2,\ 3,\ ...$) is given by:

$$\begin{aligned} \mathcal{P}^{(n+\frac{1}{2})}_{\mu_1\mu_2\ldots\mu_n,\nu_1\nu_2\ldots\nu_n} &= \sum_{\lambda} U_{\mu_1\mu_2\ldots\mu_n}(\vec{p},\lambda)\bar{U}_{\nu_1\nu_2\ldots\nu_n}(\vec{p},\lambda) \\ &= \frac{n+1}{2n+3}(\not{p}+m)\gamma^{\alpha}\gamma^{\beta}\mathcal{P}^{(n+1)}_{\alpha\mu_1\mu_2\ldots\mu_n,\beta\nu_1\nu_2\ldots\nu_n}, \end{aligned} \tag{4}$$

where

$$\mathcal{P}^{(n)}_{\mu_1\mu_2\ldots\mu_n,\nu_1\nu_2\ldots\nu_n} = \sum_{\lambda} \epsilon_{\mu_1\mu_2\ldots\mu_n}(\vec{p},\lambda)\epsilon^{*}_{\nu_1\nu_2\ldots\nu_n}(\vec{p},\lambda). \tag{5}$$

The $G^{(J^P)}$ is constructed using the projection operator and the relativistic Breit-Wigner (BW) function with a mass-dependent width, expressed as:

$$G^{(n+\frac{1}{2})} = \frac{2M_0}{M^2 - M_0^2 + iM_0\Gamma(M)} F_b \mathcal{P}^{(n+\frac{1}{2})}, \tag{6}$$

where $n = 0,\ 1,\ 2,\ ...,\ M$ is the invariant mass of $\Xi^-\pi^+$, and M_0 and $\Gamma(M)$ are the mass and width of the Ξ^{*0}, respectively. Since baryons are not point-like particles, form factors modifying the BW shape are required to describe them. We use a phenomenological form factor [**?**, **?**] for the resonance, defined as

$$F_b = \begin{cases} 1 & J = 1/2 \\ e^{-\frac{|M^2 - M_0^2|}{8M_0\Gamma}} & J = 3/2 \\ e^{-\frac{|M^2 - M_0^2|}{4M_0\Gamma}} & J = 5/2 \\ e^{-\frac{|M^2 - M_0^2|}{2M_0\Gamma}} & J = 7/2 \end{cases}. \tag{7}$$

Decay Amplitude

The total decay amplitude of the $\Xi_c^+ \to \Xi^-\pi^+\pi^+$ is calculated via:

$$M = \sum_i c_i M_i$$

c_i is the free complex parameter, usually determined by the fit to data.

M_i is the decay amplitude for the possible Ξ^* resonance.

- In this work, we use a framework called FDC (Feynman-Diagram-Calculation) [1] to automatically construct the decay amplitude used to perform a likelihood fit to data.

- FDC has been successfully applied in some partial wave analyses in BESIII experiment [2-5].

[1] J. X. Wang, Nucl. Instrum. Meth. A 534, 241 (2004).
[2] M. Ablikim et al. (BESIII Collaboration), Phys. Rev. D 110, 052006 (2024).
[3] M. Ablikim et al. (BESIII Collaboration), Phys. Rev. D 109, 072008 (2024).
[4] M. Ablikim et al. (BESIII Collaboration), Phys. Rev. Lett. 131, 151901 (2023).
[5] M. Ablikim et al. (BESIII Collaboration), Phys. Rev. D 106, 072006 (2022).

Fit Method

- The complex parameters c_i are determined using an unbinned maximum likelihood fit.
- The joint probability density for observing N events in a data set is given by

$$\mathcal{L} = \prod_{i=1}^{N} P(x_i),$$

where $P(x_i)$ is a probability to produce event i with four-vector momentum $x_i = (E,\ p_x,\ p_y,\ p_z)_i$. The $P(x_i)$ is calculated from the differential cross section as follows

$$P(x_i) = \frac{\omega(x_i)}{\int \omega(x) d\Phi},$$

where $\omega(x_i) = (d\sigma/d\Phi)_i$ is the differential cross section and $\int \omega(x) d\Phi$ is the observed total cross section. The differential cross section is given by

$$\omega(x) \equiv \frac{d\sigma}{d\Phi} = \left| \sum_j c_j M_j \right|^2 .$$

Fit Method

- For technical reasons, rather than maximizing L, the object function, $S = -\ln L$, is minimized using the MINUIT package, where

$$\mathcal{S} = -\sum_{i}^{N} \ln\omega(x_i) + N\ln\left[\int \omega(x)d\Phi\right].$$

The $\int \omega(x)d\Phi$ is evaluated using a PHSP MC sample consisting of $N_{\rm PHSP}$ events. The normalization integral is then computed as follows

$$\int \omega(x)d\Phi = \frac{1}{N_{\rm PHSP}} \sum_{k}^{N_{\rm PHSP}} \omega(x_k).$$

The background events are subtracted from the $-\ln\mathcal{L}$ function using

$$-\ln\mathcal{L} = -(\ln\mathcal{L}_{\rm data} - \omega\ln\mathcal{L}_{bkg}).$$

- The $-\ln L_{bkg}$ is constructed from the normalized background events from generic MC in Ξ_c^+ signal region.

Spin-parity determination

- A partial wave analysis is performed to the survived events passing through the event selections from Belle and Belle II. We make a simultaneous fit on Belle and Belle II datasets.
- The resonances $\Xi(1530), \Xi(1620), \Xi(1690), \Xi(1820), \Xi(1950)$, and $\Xi(2030)$ are considered in the preliminary fit, and the one with a statistical significance smaller than 3σ will be excluded in the final fit.
- The non-resonant process is also considered in the fit.
- The J^P assignments $1/2^{\pm}$, $3/2^{\pm}$, $5/2^{\pm}$, and $7/2^{\pm}$ for each resonance are tested in the fit. The $J > 7/2$ are excluded due to the fact that high spin is depressed by the Barrier factor.
- **The J^P hypothesis with the smallest S value from the fit is selected as the favored J^P assignment.**

A likelihood ratio t is used as a test variable to discriminate between the favored J^P hypothesis ($J^P_{\rm fav}$) and the alternative J^P hypotheses ($J^P_{\rm alt}$), calculated as

$$t \equiv -2\ln\left[\mathcal{L}(J^P_{\rm alt})/\mathcal{L}(J^P_{\rm fav})\right]$$

- To quantify the discriminating power of J^P_{fav} over J^P_{alt}, a statistical significance is estimated by
  - $<t>$ and $\sigma(t)$ are the mean and standard deviation under the J^P_{alt} hypothesis.
  - The t_{data} is the t value from data.

If $T > 5\sigma$, we think the discrimination is strong.

Toy MC generation

We construct the effective Lagrangian of the $\Xi_c^+ \to \Xi^-\pi^+\pi^+$ decay using FDC from a very simple input values.

Then we generate the toy MC simulated events from the FDC.

We take the $\Xi(1620)$ as an example. The mass and width are taken from the central values of the PDG [1], which are $M = 1.62$ GeV/c^2 and $\Gamma = 32$ MeV, respectively. Then we generate 100,000 $\Xi_c^+ \to \Xi(1620)\pi^+$; $\Xi(1620) \to \Xi^-\pi^+$ toy MC events according the decay amplitude under different J^P hypotheses and compare the invariant mass distributions of $\Xi^-\pi^+$, helicity angular distributions of Ξ^*, and Dalitz plots from these toy MC events, which are shown in Figs. 3, 4, 5, 6. The θ_{Ξ^*} is the helicity angle of Ξ^*, which is defined as the angle between the Ξ^- momentum vector in the Ξ^* rest frame and the opposite of the Ξ_c^+ momentum vector in the laboratory frame.

Toy MC generation

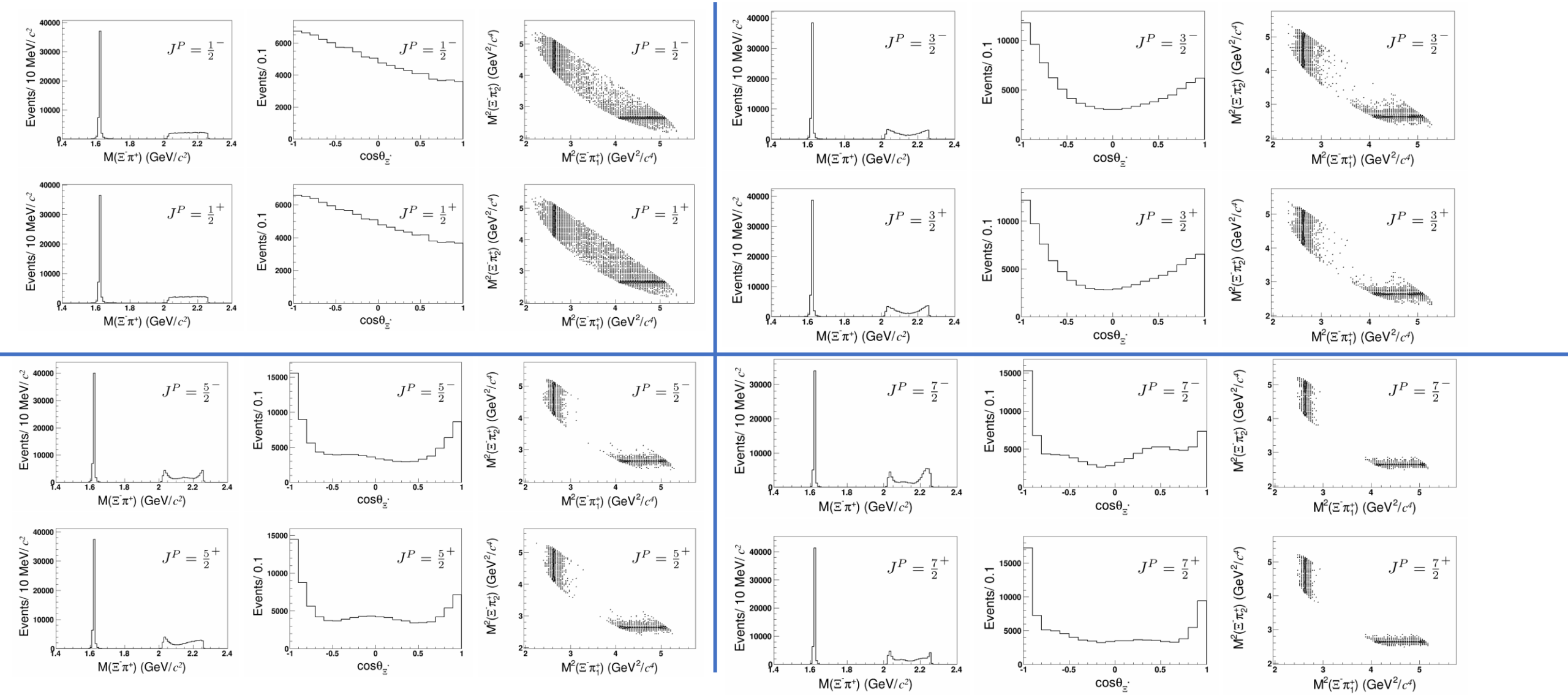

By comparison, we see the mass, angular, and Dalitz distributions under different spin hypotheses are distinguishable
However, they are not be significantly distinguished by parity.

Toy MC generation

By comparison, we see the mass, angular, and Dalitz distributions under different spin hypotheses are distinguishable
However, they are not be significantly distinguished by parity.

This is because:

(1) The effective vertices of the $\Xi_c^+ \to \Xi^*\pi^+$ and $\Xi^* \to \Xi^-\pi^+$ **differ much for different Spin**.

(2) The effective vertices of the $\Xi_c^+ \to \Xi^*\pi^+$ **are identical for parity $P = \pm 1$**

TABLE II. Effective vertices $\Xi_c^+(p) - \Xi^{*0}[J^P] - \pi^+(p_1)$ and $\Xi^{*0}[J^P] - \Xi^-(p_2) - \pi^+(p_3)$ with the $J^P = \frac{1}{2}^-, \frac{1}{2}^+, \frac{3}{2}^-, \frac{3}{2}^+, \frac{5}{2}^-, \frac{5}{2}^+, \frac{7}{2}^-$, and $\frac{7}{2}^+$. The $f_{i(i=1,2,3,\ldots)}$ is the complex parameter, usually determined by the fit to data. The μ, ν, α, and β are the Lorentz indexes.

J^P	$\Xi_c^+(p) - \Xi^{*0} - \pi^+(p_1)$	$\Xi^{*0} - \Xi^-(p_2) - \pi^+(p_3)$
$\frac{1}{2}^-$	$f_1\gamma_5 i + f_2$	f_3
$\frac{1}{2}^+$	$f_4\gamma_5 i + f_5$	$f_6\gamma_5 i$
$\frac{3}{2}^-$	$f_7 p_\mu i + f_8\gamma_5 p_\mu$	$f_9\gamma_5 p_{2\alpha}$
$\frac{3}{2}^+$	$f_{10} p_\mu i + f_{11}\gamma_5 p_\mu$	$f_{12} p_{2\alpha} i$
$\frac{5}{2}^-$	$f_{13} p_\mu p_\nu + f_{14}\gamma_5 p_\mu p_\nu i$	$f_{15} p_{2\alpha} p_{2\beta}$
$\frac{5}{2}^+$	$f_{16} p_\mu p_\nu + f_{17}\gamma_5 p_\mu p_\nu i$	$f_{18}\gamma_5 p_{2\alpha} p_{2\beta} i$
$\frac{7}{2}^-$	$f_{19} p_\mu p_\nu p_\sigma i + f_{20}\gamma_5 p_\mu p_\nu p_\sigma$	$f_{21}\gamma_5 p_{2\alpha} p_{2\beta} p_{2\tau}$
$\frac{7}{2}^+$	$f_{22} p_\mu p_\nu p_\sigma i + f_{23}\gamma_5 p_\mu p_\nu p_\sigma$	$f_{24} p_{2\alpha} p_{2\beta} p_{2\tau} i$

Toy MC generation

We construct the effective Lagrangian of the $\Xi_c^+ \to \Xi^-\pi^+\pi^+$ decay using FDC from a very simple input values.

We list the input properties of the possible Ξ^* states:

- Masses and widths from PDG
- J^P of $\Xi(1530/1820)$ from PDG;
- J^P of $\Xi(1690)$ from BESIII result [PRD109, 072008 (2024).]
- J^P of $\Xi(1620/1950/2030)$ from theo. predictions.

The nonresonant process of the $\Xi_c^+ \to \Xi^-\pi^+\pi^+$ is also considered via the PHSP model.

We also tested alternative J^P beyond those specified in Table and find the choice of input J^P values does not significantly impact the final conclusions.

We list assumed ratios for each resonance and the corresponding interference ratios between pairs of resonances. These ratios are determined based on the $M(\Xi^-\pi^+)$ spectrum from previous Belle published result.

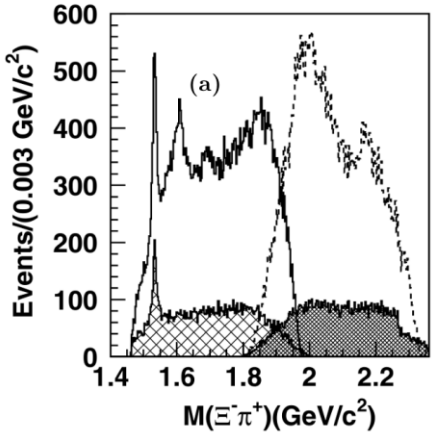

TABLE III. The input properties of the Ξ^{*0} states.

Resonance	Mass (MeV/c^2)	Width (MeV)	J^P
$\Xi(1530)^0$	1531.8	9.1	$\frac{3}{2}^+$
$\Xi(1620)^0$	1620.0	32.0	$\frac{1}{2}^-$
$\Xi(1690)^0$	1690.0	20.0	$\frac{1}{2}^-$
$\Xi(1820)^0$	1823.0	24.0	$\frac{3}{2}^-$
$\Xi(1950)^0$	1950.0	60.0	$\frac{1}{2}^-$
$\Xi(2030)^0$	2025.0	20.0	$\frac{5}{2}^-$

TABLE IV. Assumed ratio of each resonance and the corresponding interference term between two resonances (in %).

Ratio	$\Xi(1530)^0$	$\Xi(1620)^0$	$\Xi(1690)^0$	$\Xi(1820)^0$	$\Xi(1950)^0$	$\Xi(2030)^0$	nonresonance
$\Xi(1530)^0$	5.4	0.0	0.0	0.0	0.0	0.1	−0.2
$\Xi(1620)^0$		1.3	0.1	0.0	−0.1	0.0	1.4
$\Xi(1690)^0$			0.7	0.0	0.0	0.0	1.1
$\Xi(1820)^0$				2.8	−0.6	0.0	0.1
$\Xi(1950)^0$					9.0	0.0	−0.8
$\Xi(2030)^0$						1.5	0.0
Nonresonance							79.3

Fit to Toy MC samples

- Using the above properties as the input parameters, we generate toy MC samples according to the amplitude through the sampling method.

- Then we perform an unbinned maximum likelihood fit to the toy MC samples.
  - The mass, width, and ratio of each resonance are floated.
  - All J^P assignments are tested for each resonance in the fit.

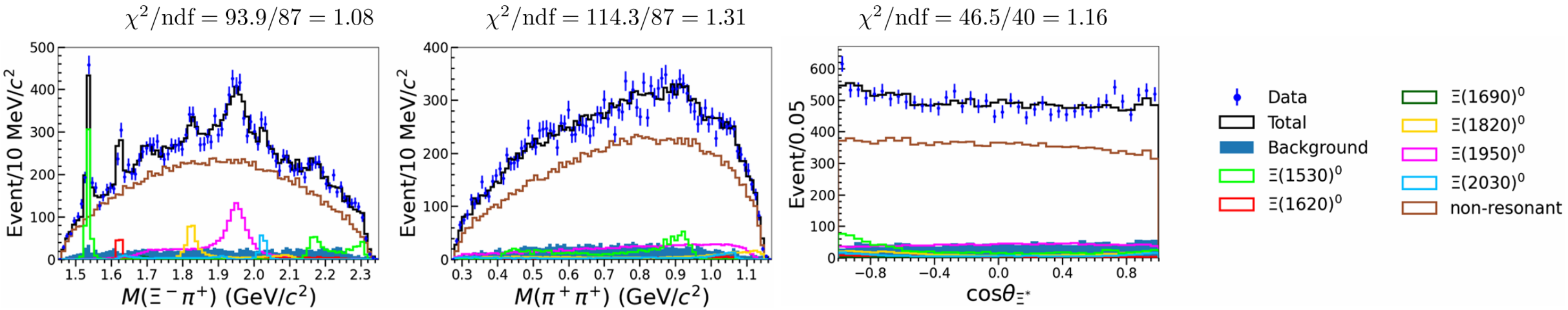

Best PWA fit results for one toy MC sample

Consistency of Input and Output

- Five hundred sets of toy samples are generated, each with the same size as described above.
- We fit these sets of toy samples and extract the **ratios, masses, and widths.**

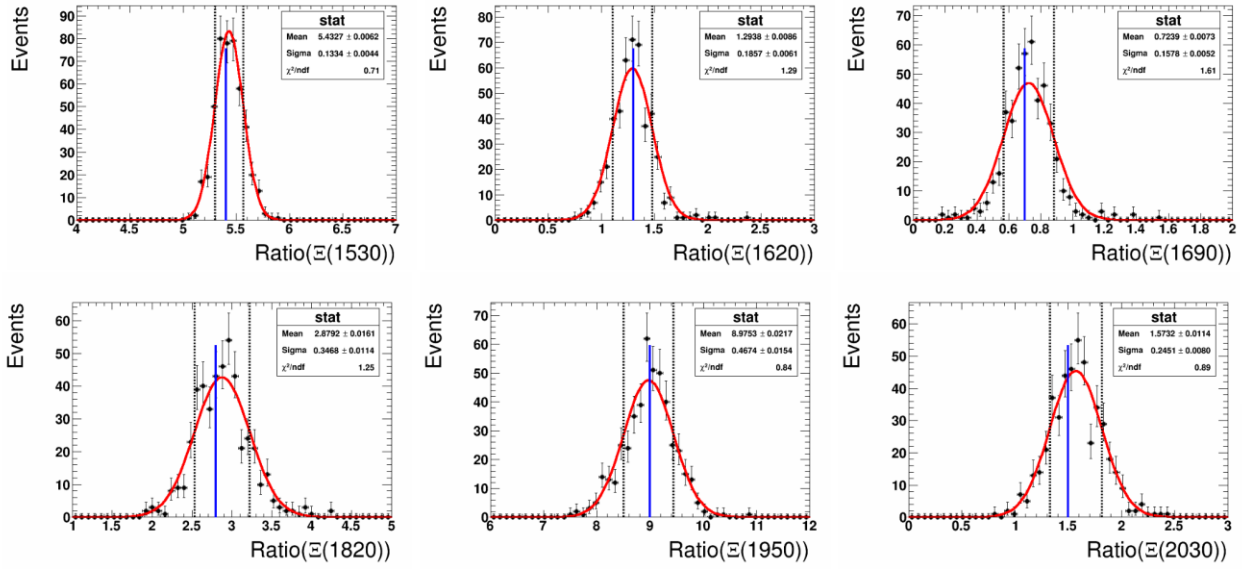

Figure 8: The distributions of each resonance ratio. The red curves are the Gaussian functions; The two black dashed lines correspond to $\pm 1\sigma$, and the blue lines represent the input ratios.

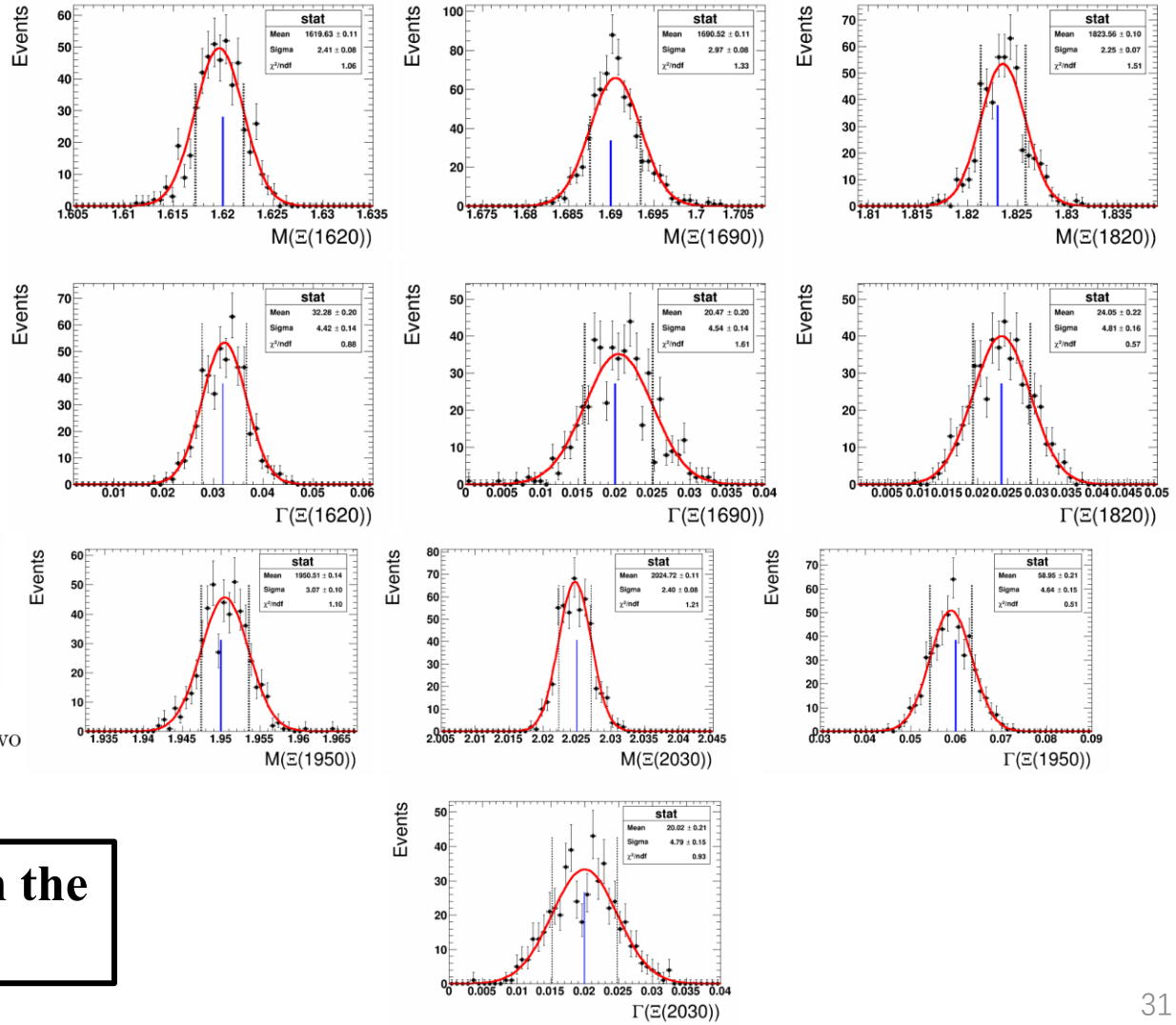

The fitted ratio, mass, and width are consistent with the input values.

Spin-parity determination

- The J^P assignments $1/2^{\pm}$, $3/2^{\pm}$, $5/2^{\pm}$, and $7/2^{\pm}$ are considered in the fit for the resonance.
- The minimum log-likelihood (LL) values are determined for each J^P hypothesis, and the one with the smallest LL is selected as the favored J^P assignment.
- **The favored J^P from the fit is consistent with the input one for each resonance.**

We perform a t-test to quantify the discriminating power of favored J^P_{fav} over alternative J^P_{alt}.

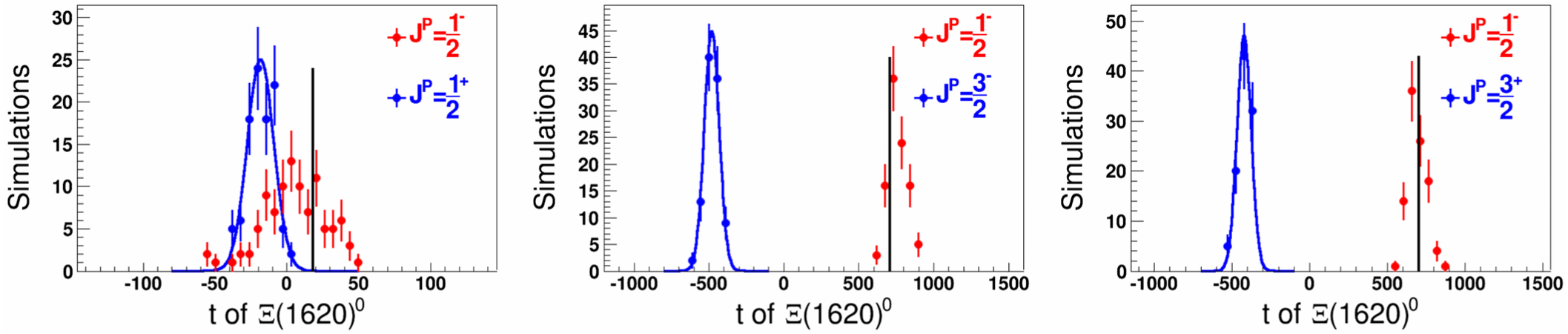

FIG. 3. Distributions of the test statistic t for the $\Xi(1620)^0$, for simulated experiments under the $J^P_{\rm alt} = \frac{1}{2}^+, \frac{3}{2}^-$, and $\frac{3}{2}^+$ hypotheses (blue histograms) and the $J^P_{\rm fav} = \frac{1}{2}^-$ hypothesis (red histograms). The values of the test statistics for the toy data, $t_{\rm toydata}$, are shown by the solid vertical lines. The curves show the Gaussian fits to the distributions of the left peaks.

Spin-parity determination

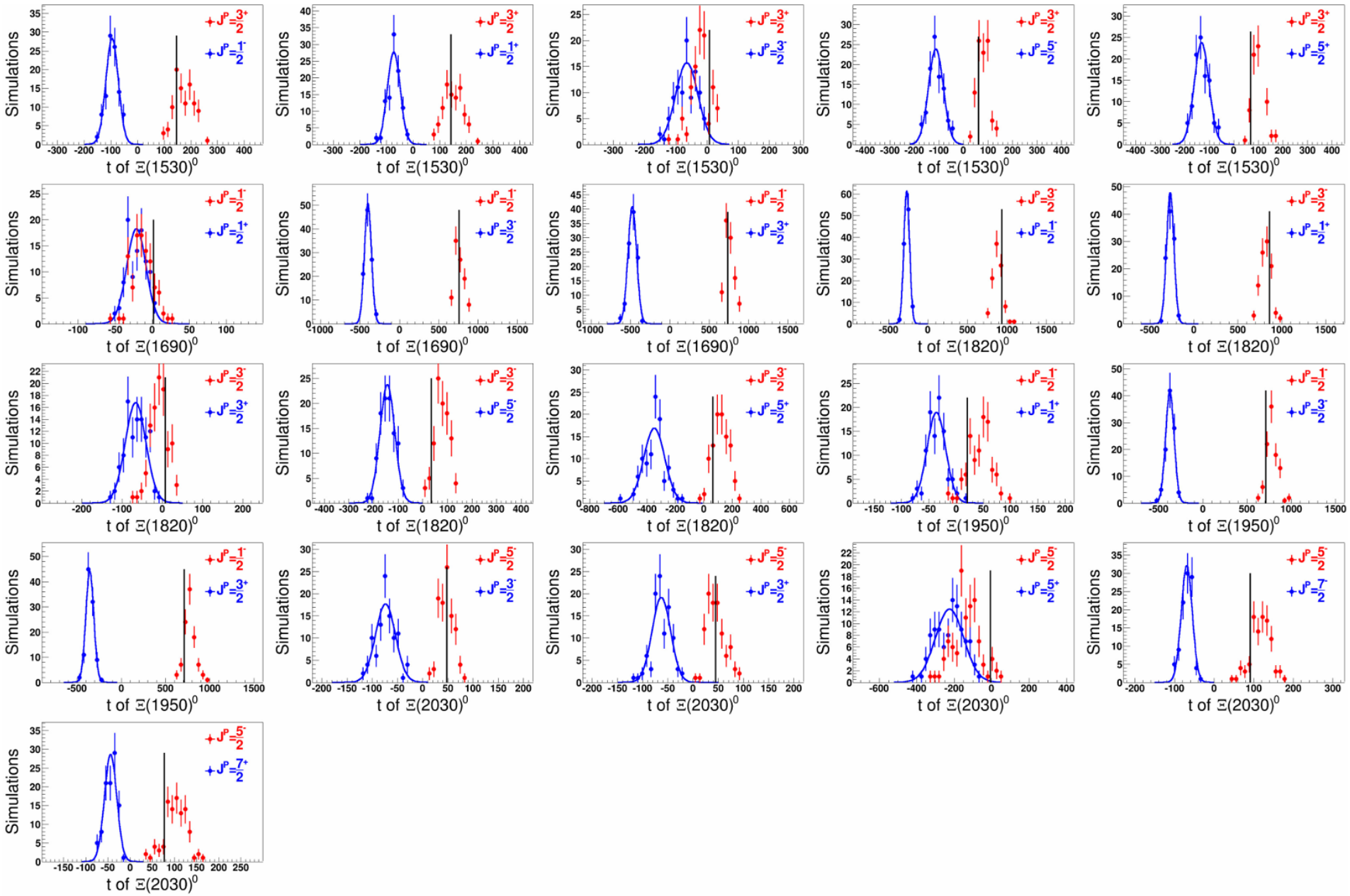

Spin-parity determination

A statistical significance for rejecting the alternative J^P_{alt} hypothesis in favor of favored J^P_{fav} hypothesis is calculated and listed.

TABLE V. The significances of rejection of $J^P_{\rm alt}$ for each resonance.

		$J^P_{\rm alt}$							
Resonance	$J^P_{\rm fav}$	$\frac{1}{2}^-$	$\frac{1}{2}^+$	$\frac{3}{2}^-$	$\frac{3}{2}^+$	$\frac{5}{2}^-$	$\frac{5}{2}^+$	$\frac{7}{2}^-$	$\frac{7}{2}^+$
$\Xi(1530)^0$	$\frac{3}{2}^+$	10.0σ	9.0σ	2.0σ	...	5.8σ	6.6σ	...	...
$\Xi(1620)^0$	$\frac{1}{2}^-$	...	3.9σ	22.4σ	24.5σ	...	...	...	...
$\Xi(1690)^0$	$\frac{1}{2}^-$	...	1.8σ	24.3σ	22.1σ	...	...	...	...
$\Xi(1820)^0$	$\frac{3}{2}^-$	28.0σ	26.5σ	...	2.8σ	5.8σ	5.7σ	...	...
$\Xi(1950)^0$	$\frac{1}{2}^-$	...	3.2σ	23.3σ	23.8σ	...	...	...	...
$\Xi(2030)^0$	$\frac{5}{2}^-$	...	...	6.3σ	6.0σ	...	2.9σ	11.6σ	8.7σ

Using the current Belle integrated luminosity, we find

- the discrimination power between different spin states exceeds 5σ in all tested spin configurations.
- the discrimination power for distinguishing between different parity states with the same spin is relatively weaker.

Spin-parity determination

This is because:

(1) the effective vertices for $\Xi_c^+ \to \Xi^{*0}\,\pi^+$ are identical for $P = \pm 1$;

(2) the statistical sample size of the resonance affects the ability to discriminate between $P = \pm 1$ states with the same spin.

- To study the effect of statistical sample size on parity determination, we increased the toy MC sample statistics by 5 and repeated the analysis. The PWA results show that the rejection significance exceeds 5σ for $P = \pm 1$ when we increase the data size.

Resonance	J^P_{alt} over J^P_{fav}	Rejection Significance
$\Xi(1530)^0$	$3/2^-$ over $3/2^+$	7.9σ
$\Xi(1620)^0$	$1/2^+$ over $1/2^-$	13.2σ
$\Xi(1690)^0$	$1/2^+$ over $1/2^-$	8.5σ
$\Xi(1820)^0$	$3/2^+$ over $3/2^-$	6.7σ
$\Xi(1950)^0$	$1/2^+$ over $1/2^-$	9.6σ
$\Xi(2030)^0$	$5/2^+$ over $5/2^-$	8.8σ

- Under limited statistics, the primary challenge in parity determination arises from the identical effective vertices of the $\Xi_c^+ \to \Xi^{*0}\,\pi^+$ decay for both $P = \pm 1$ hypotheses.
- However, the effective vertices of the subsequent decay $\Xi^{*0} \to \Xi^-\pi^+$exhibit distinguishable behavior for $P = \pm 1$, enabling the model to perform parity determination effectively under large statistics.

Systematic uncertainty

Table 11: Sources of the systematic uncertainty (in unit of %). Uncertainties less than 0.5% are considered negligible. The range in the table is for different Ξ^* states and the specific values are written below.

Sources	Belle	Belle II
Tracking	1.6	1.7
PID	0.02	0.01
Λ reconstruction	1.8	0.9
MC statistic	0.2	0.2
Weight factor	0.01−0.4	0.01−0.4
Form factor	1.0−8.2	1.0−8.2
Detector resolution	1.1−3.8	1.1−3.8
Total	3.1−9.0	2.8−8.8

The background contribution is controlled by the background events in the Ξ_c^+ signal region from generic MC samples. The weight factor $\omega = N_{\rm bkg}^{\rm data}/N_{\rm bkg}^{\rm MC}$ accounts for the difference on the number of background events between generic MC samples and data, which are $\omega = 0.45\pm0.03$ for Belle and $\omega = 1.40\pm0.11$ for Belle II. In the fit, the ω is fixed to the central value. We change it by $\pm1\sigma$ to evaluate the systematic uncertainty. The maximum difference on the fitted ratios of each resonance are taken as the conservative systematic uncertainty, which is negligible ($< 1\%$). Once we open the box, we will repeat this procedure on data.

Systematic uncertainty

- We modified the form factor to the one used in [PRD 109, 072008 (2024)] to estimate the uncertainty from the different form factor choices.

$$F_b = \begin{cases} 1 & J = \frac{1}{2} \\ e^{-\frac{|M^2 - M_0^2|}{2^{(4-n)} M_0 \Gamma}} & J = \frac{1}{2} + n \end{cases} \rightarrow F_b = \begin{cases} \frac{16}{16 + |M^2 - M_0^2|} & J = \frac{1}{2} \\ e^{-\frac{|M^2 - M_0^2|}{4}} & J = \frac{1}{2} + n \end{cases}$$

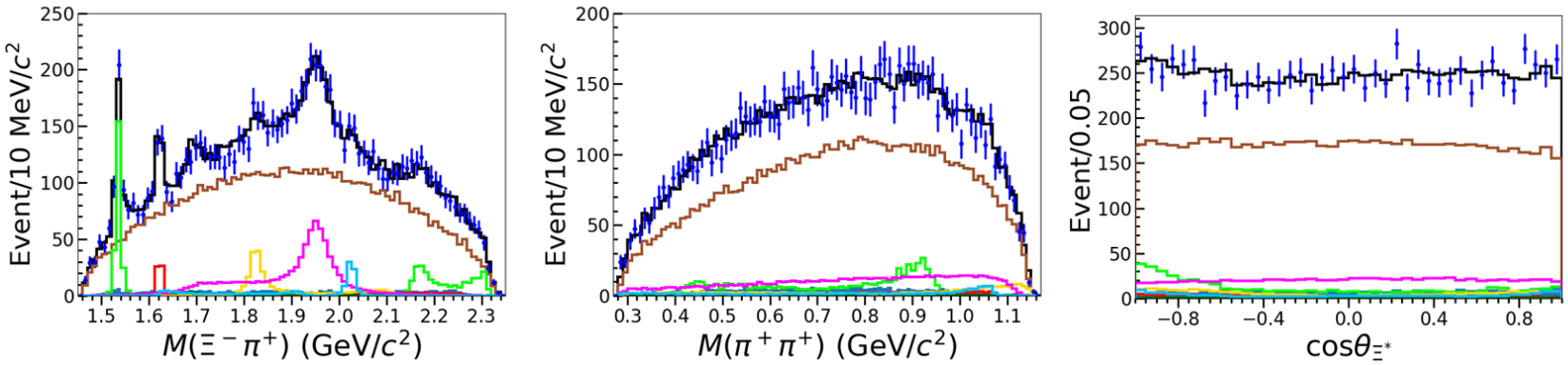

Table 12: Fitted ratios of each resonance under different form factors (in unit of %).

Resonance	Nominal form factor	New form factor	Difference
$\Xi(1530)^0$	5.43 ± 0.14	5.62 ± 0.13	3.5%
$\Xi(1620)^0$	1.30 ± 0.19	1.21 ± 0.18	6.9%
$\Xi(1690)^0$	0.73 ± 0.16	0.67 ± 0.16	8.2%
$\Xi(1820)^0$	2.86 ± 0.36	2.89 ± 0.33	1.0%
$\Xi(1950)^0$	8.94 ± 0.49	9.13 ± 0.51	2.1%
$\Xi(2030)^0$	1.55 ± 0.26	1.47 ± 0.25	5.2%

Summary and Plan

- B2N: https://docs.belle2.org/files/4567/BELLE2-NOTE-PH-2025-035/2/BELLE2-NOTE-PH-2025-035.pdf

- **Next to do**
  - RC review.
  - Wait for opening box

Thanks for your attention!

Backup